CARBON 77 (2014) 208–214

Available at www.sciencedirect.com

ScienceDirect

journal homepage: www.elsevier.com/locate/carbon

Spin-polarized bandgap of graphene induced by alternative chemisorption with MgO (111) substrate

Sung Beom Cho, Yong-Chae Chung *

Department of Materials Science and Engineering, Hanyang University, Seoul, Republic of Korea

ARTICLE INFO

Article history:
Received 23 December 2013
Accepted 9 May 2014
Available online 27 May 2014

ABSTRACT

Using First-principle calculations, the substrate effect of O-terminated $(\sqrt{3} \times \sqrt{3})$ MgO (111) on graphene was investigated for spintronics application. It was found that the graphene could be turned into a spin-polarized semiconductor due to alternative sp3 chemisorption with the substrate. The majority spin channel has an insulating band gap of 2 eV, while the minority spin channel has a semiconducting band gap of 0.3 eV. These results imply that the graphene with a tailored pattern of chemisorption could be highly efficient for introducing a totally spin-polarized current and controlling its on/off switching.

1. Introduction

Spintronics, solid state devices based on spin-dependent electron transport, has huge advantages for nonvolatile information processing with low-power-consumption [1,2]. In the field of spintronics, graphene is expected to produce breakthroughs, due to its long spin lifetime and high mobility [3]. In particular, the length of spin coherence length in graphene can reach the micrometer range at room temperature indicating very appealing prospects for designing spintronics [4]. There are still unresolved bottlenecks related to spin filtering that would have to be addressed in order to realize graphene-based spintronics. One method to induce a spin-polarized current on the graphene is using the magnetoresistance effect between two magnetic electrodes [5–7]. Despite the large difference in resistivity between the two spin directions in the magnetoresistance device, this method is not efficient enough for a totally polarized spin [8]. A promising alternative method is introducing half-metallicity to graphene by employing a zigzag nanoribbon structure with an electric field [9]. However, this strategy requires a strongelectric field that is impractical for real devices. New strategies have been proposed to solve this problem, such as edge modification of the nanoribbon [10,11], hydrogen patterning [12], and B/N doping [13,14]. Although these strategies successfully predicted the half-metallicity, a bottleneck still remains for spin-filtering due to the experimental difficulty associated with achieving fine control of the edge modification, adsorbate patterning, and doping in graphene nanoribbons. Intensive studies are still required to achieve a feasible method of introducing a totally spin-polarized current to graphene.

Magnetic semiconductors are the best-suited materials not only for spin-filtering but also for diverse spintronics applications [15,16,1,2]. Magnetic semiconductors exhibit both ferromagnetism and semiconductor properties, which have a huge advantage in controlling both the spin-current and the charge-current. For this reason, it has great potential for applications such as spin-polarized light-emitting diodes (spin-LEDs) and spin-polarized field-effect transistors (spin-FETs) [17]. Furthermore, the most important advantage of

* *Corresponding author.*
E-mail address: yongchae@hanyang.ac.kr (Y.-C. Chung).
http://dx.doi.org/10.1016/j.carbon.2014.05.023
0008-6223/

magnetic semiconductors as potential application is their easy integration into current semiconductor devices. For example, electrical spin injection into (Ga,Mn) As has enabled to the realization of the spin-polarized optoelectronics [18–21]. The advances of creation and control of spin in silicon are also expected to open a new way of spin-based information technology [22,23]. Those implementations of spin functionality are achieved by the defect and interface engineering, which is based on the low-temperature effect. Therefore, there have been intensive efforts to find out suitable magnetic semiconducting materials that have thermal stability and an appropriate bandgap [24–26]. In this direction, it would be highly desirable to introduce magnetic semiconducting properties to graphene by tuning its intrinsic band structure, as the half-metallicity is introduced to graphene.

Tuning the properties of graphene via substrate treatment has obvious technological advantages due to its simple process. MgO has been extensively used material for spin-filtering [27,28], and shows outstanding performance in spin-filtering as a tunneling barrier [29,30]. A significant advantage of using MgO in spin filtering is the ability to apply it using a simple deposition process such as sputtering or evaporation [31,27]. Recently, Kelber et al. achieved direct deposition of graphene onto an MgO (111) polar surface, and observed bandgap opening of the graphene [32]. It was theoretically predicted that periodic chemisorption between graphene and an MgO (111) substrate can induce the bandgap of graphene [33]. These studies imply that the strong interaction between graphene and a MgO (111) substrate results in the modification of the electronic structure of the graphene. Fortunately, the MgO (111) polar surface is prone to be reconstructed into various surface structures because of its surface polarity from its rocksalt structure [34,35]. In furthering this, it is possible that the electronic structure of graphene can be tuned with an oxygen-terminated $(\sqrt{3}\times\sqrt{3})$ MgO (111) phase, which is one of the experimentally observable reconstruction structures of MgO (111) under dry conditions [34,36,37].

In this study, it was found that the interface interaction between graphene and $(\sqrt{3}\times\sqrt{3})$ reconstructed MgO (111) results in a magnetic semiconducting property using Density Functional Theory. Remarkably, a spin-polarized bandgap was observed, which holds significant technical importance for the realization of spintronics. Furthermore, the spin-polarized bandgap is shown to result from the substrate effect of $(\sqrt{3}\times\sqrt{3})$ the reconstructed MgO (111) surface.

2. Calculation details

Graphene on MgO (111) was described using symmetric slab models to avoid the effect of the internal dipole moment caused by the polarity of the MgO (111) surface. The MgO (111) surface consists of 13 symmetric layers and the three central slab layers, which were kept fixed within the structural parameter of the bulk MgO. The two layers of graphene were then adsorbed on both side of surfaces of the MgO (111) with the corresponding periodicity of the reconstructed MgO (111) structure. At least 12 Å of vacuum distance was chosen for the slab model to avoid interference with the supercell. All DFT calculations on the supercell were performed with the Vienna *ab initio* simulation package (VASP) code [38], with implementation of the Perdew–Burke–Ernzerhof exchange correlation function [39]. The projector augmented wave (PAW) method [40] was employed to describe the interactions of the valence electrons with their atomic cores. Throughout, a plane-wave basis set was employed to describe a valence electron with a kinetic energy cutoff of 450 eV. All the interface structures were fully relaxed until the maximum total Hellmann–Feynmann force was less than 0.02 eV/Å. The van der Waals (vdW) force was described using the semiempirical correction scheme of Grimme (DFT-D2) [41]. Though the DFT-D2 method can underestimate the binding energy of ionic systems [42,43], it has successfully predicted the geometries of graphene-related structures [44,45]. The [46] $(3\times3\times1)$ k-point grid was used for structural optimizations, and a $(7\times7\times1)$ grid was used to obtain the electronic band structures in the (2×2) coincidence unit cell. The atomic charges were estimated by integrating the charge densities over cells with a Wigner–Seitz radius. The other calculation details can be seen in a previous study of graphene on a octo-polar MgO (111) polar surface [33].

3. Results and discussion

The structure of $(\sqrt{3}\times\sqrt{3})$ MgO (111) is comprised of O-terminated surfaces with 1/3 of the bulk-like O ions missing. The $(\sqrt{3}\times\sqrt{3})$ MgO (111) has 5.19 Å of periodicity, which can form a coincidence lattice with (2×2) unitcell of graphene with a 5% strain. The 5% strain of the graphene seems unstable at the interface, but there is sufficient possibility to form an interface with $(\sqrt{3}\times\sqrt{3})$ MgO (111). In the case of graphene on 6H-SiC, even though it has an 8% lattice mismatch at the interface, the interface structure can exist stably [47,48]. This is due to the dense chemisorption between graphene and 6H-SiC, which overcompensates for the elastic stress at the interface. Even if the elastic stress becomes more dominant and induces corrugation under certain conditions, the chemisorped interface structure still remains, and significantly contributes to the entire electronic structure of graphene. Similarly, graphene on $(\sqrt{3}\times\sqrt{3})$ MgO (111) can stably exist if the contribution of the interface interaction is more dominant than the elastic strain. To determine the stability, the interface energy was calculated. The interface energy was defined as the energy difference between the graphene/MgO (111) and the sum of pristine graphene and the separated MgO (111) substrate as follows:

$$E_{\text{interface}} = E_{\text{graphene/MgO}} - E_{\text{graphene}} - E_{\text{MgO}} \quad (1)$$

The obtained interface energy was −0.3 eV per coincidence unit cell, which indicates that the interface structure is more stable. However, it should be noted that the obtained interface energy includes the DFT-D2 term, which underestimates the vdW energy of the ionized oxygen. This indicates that the strain energy of graphene can be sufficiently released by the chemisorption at the interface, and graphene can be stably placed on $(\sqrt{3}\times\sqrt{3})$ MgO (111). To ensure the stability of the interface, non vdW DFT calculations were also performed as a comparison. The interface energy, which did not consider

the vdW energy, was −0.01 eV per coincidence unit cell. The result indicates that graphene can stably exist on the lattice mismatched MgO (111) substrate with small vdW interaction.

Fig. 1(a) shows the interface structure of graphene on $(\sqrt{3}\times\sqrt{3})$ MgO (111). When graphene was adsorbed on the $(\sqrt{3}\times\sqrt{3})$ MgO (111) surface, half of the surface oxygen ions were occupied. A carbon atom on top of the occupied surface oxygen moved down to 0.4 Å and a charge transfer occured, as shown in Fig. 1(b). A charge of 0.21*e* was transferred to the surface oxygen ions, which indicates that chemisorption is formed at the interface. It is expected that the chemisorption would greatly contribute to releasing the strain energy of the graphene on the MgO (111). When the interface was introduced to the graphene, an unexpected magnetic ordering of graphene was observed. The graphene, which was originally a non-magnetic material became ferrimagnetic on the substrate as shown in Fig. 2. The observed ferrimagnetism was induced by the ordering of the magnetic moment of each sublattice of the graphene. One sublattice, which occupies the surface oxygen showed −0.06 μ_B (small downward arrow in Fig. 2) and the other sublattice showed 0.17 μ_B (large upward arrow in Fig. 2). This magnetic ordering implies that the band

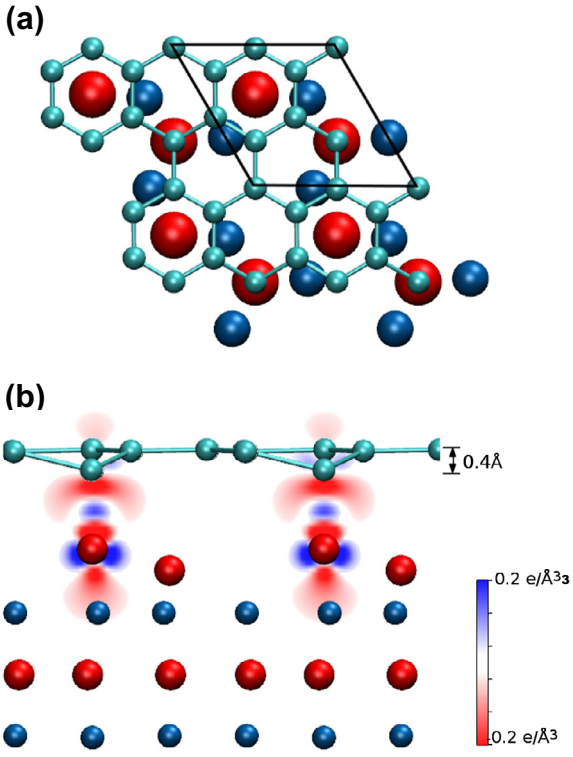

Fig. 1 – (a) Topview of the graphene on $(\sqrt{3}\times\sqrt{3})$ MgO (111). The cyan, red and blue balls represent the C, O, and Mg atoms, respectively. The black parallelogram indicates the coincidence unit cell of the graphene and the substrate. (b) The sideview and charge density difference of the graphene on $(\sqrt{3}\times\sqrt{3})$ MgO (111). Small corrugation occurs due to the carbon atom on the oxygen ion, which moved down to 0.4 Å. Then, a large charge transfer occurred between the interface, which indicates that the adhesion character is chemisorption. (A colour version of this figure can be viewed online.)

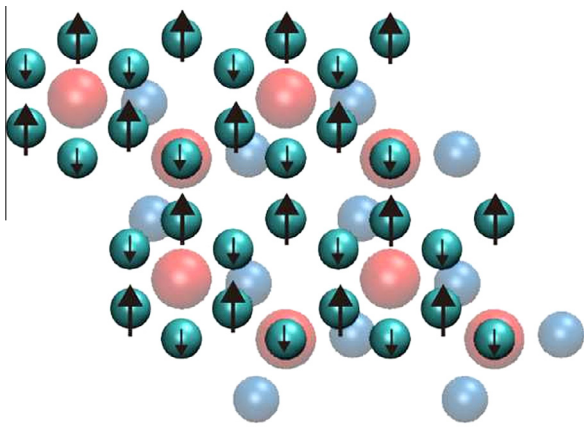

Fig. 2 – The magnetic moment of the graphene on $(\sqrt{3}\times\sqrt{3})$ MgO (111). Ferrimagnetism was observed in the graphene. One sublattice, which has a bond with the surface oxygen, showed a large positive magnetic moment, while the other sublattice showed a small negative magnetic moment. (A colour version of this figure can be viewed online.)

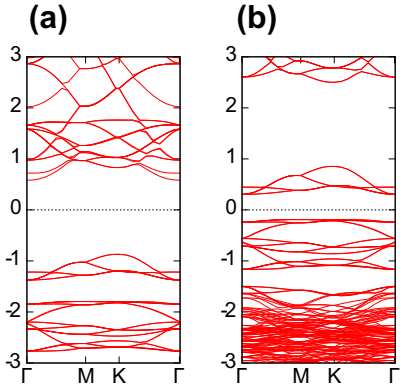

Fig. 3 – The spin-resolved band structure of the graphene on $(\sqrt{3}\times\sqrt{3})$ MgO (111). (a) The bands of the majority-spin showed an insulating property with 2.0 eV of large bandgap, while (b) the bands of the minority-spin have semiconducting 0.3 eV of semiconducting bandgap. (A colour version of this figure can be viewed online.)

structure of the graphene on the MgO (111) surface is spin-polarized.

For further investigation of the electronic structure of the graphene on the $(\sqrt{3}\times\sqrt{3})$ MgO (111), the spin-resolved band structure was calculated. A magnetic semiconducting property was observed due to the spin-polarized bandgap as shown in Fig. 3. In the majority-spin channel, there was a very large bandgap of 2 eV, which showed insulating properties. On the other hand, in the minority-spin channel, there was 0.3 eV of semiconducting bandgap. Such a spin-polarized band structure demonstrates the significant technical importance in the generation of a spin-polarized current and its on/off switching. Because of the bandgap in the minority-spin channel, the charge transport of the graphene can be controlled by an external electric field, and the current flow should be fully spin-polarized. Furthermore, a spin-polarized

band structure is obtained without transition metals or external stimuli, so it has technical advantages for the fabrication processes [49,50].

To further understand the physical origin of the substrate-induced ferrimagnetism, the electronic structure of the substrate, the isolated $(\sqrt{3}\times\sqrt{3})$ MgO (111), was investigated. As shown in Fig. 4, MgO (111) showed two different spin-states, the non-magnetic state (NM) and the ferromagnetic state (FM). Conductivity was observed in both states. The conductivity of the substrate is contributed by the surface oxygen that lost its coordination at the surface. In other words, a hole is injected in the surface oxygen, because fewer electrons are transferred from the cation. It is reported that the injected hole stays in the *2p* orbital and can be spin-polarized depending on the charged state of the surface oxygen [51]. The atomic charges of the surface oxygen in FM-MgO and NM-MgO were very similar. The valence electrons of the surface oxygen in FM-MgO (111) and NM-MgO were 6.89*e* and 6.93*e*, respectively. On the $(\sqrt{3}\times\sqrt{3})$ MgO (111) surface, the injected hole can exist in either spin-polarized state, FM or NM. It is believed that the existence of both spin states is because of the similar atomic charges of the surface oxygen. Between the two spin-states, NM-MgO (111) is slightly more stable than FM-MgO (111) by 0.15 meV per coincidence unit cell, according to our calculation.

However, when the interface junction is formed, the spin-state of the substrate is drastically changed. Fig. 5(a) shows the DOS of the supercell and the projected density of states (PDOS) of the substrate. The PDOS of the substrate indicates that the substrate shows the ferromagnetic property. The PDOS of the substrate is closer to the −1 eV shifted DOS of the FM-MgO (111) than to that of NM-MgO (111), though new states were formed near the Fermi level. This implies that the substrate, which showed a non-magnetic property

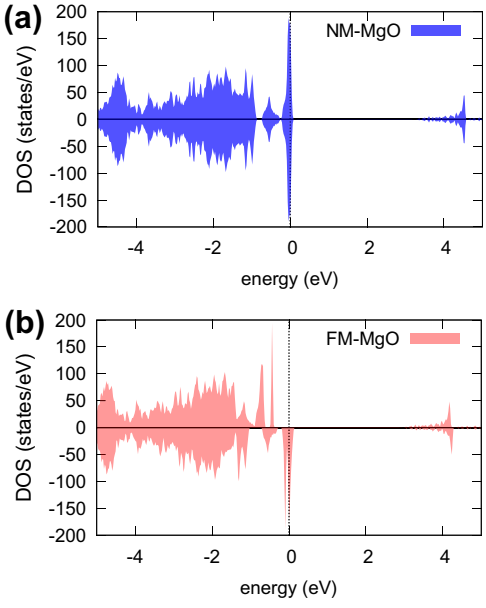

Fig. 4 – The Density of state of the isolated substrate. The $(\sqrt{3}\times\sqrt{3})$ MgO (111) showed two spin states, (a) nonmagnetic state (NM-MgO) and (b) ferromagnetic (FM-MgO). (A colour version of this figure can be viewed online.)

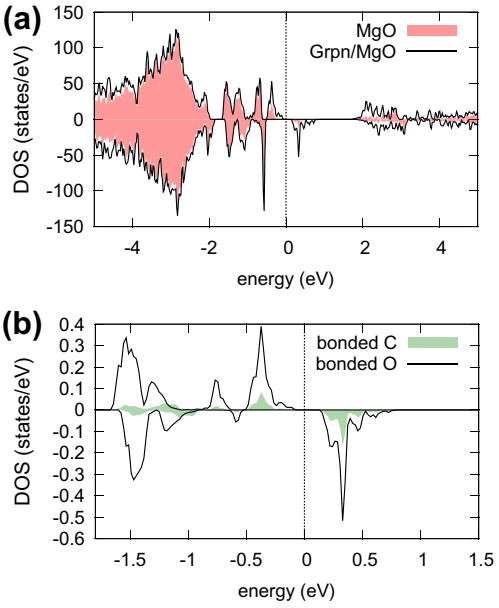

Fig. 5 – The PDOS of the graphene/MgO (111). (a) Shows the PDOS of the substrate in the graphene/MgO (111). When the interface is formed, the substrate became ferromagnetic. (b) Shows the PDOS of the carbon atom and the oxygen atom in the C–O bonding at the interface. Thd DOS of the carbon is hybridized with the oxygen, which indicates that the carbon has an additional covalent bond. (A colour version of this figure can be viewed online.)

in the ground state, became ferromagnetic due to the interface effect. The non-magnetic spin-state in the substrate was no longer observed after the interface was formed. This change indicates that there was a spin-state transition in the substrate. The magnetic moment of the surface oxygen of the ferrimagnetic interface was 0.16 μ_B, which was less than that of FM-MgO (111). A more detailed change in the magnetic moment value of the other atoms is summarized in Table 1. It is deduced that the reduced magnetic moment of the substrate at the interface results from the change of the DOS and a charge transfer from the graphene. Due to the charge transfer, the bonded surface oxygen gained 0.2*e* and the non-bonded oxygen gained 0.07*e*. It is believed that interaction with graphene should play a dominant role in the spin-polarization of the interface.

In addition to the charge transfer, covalent bonding was also found in the graphene/MgO (111) interface. Fig. 5(b) shows that the DOS of the carbon atom in the graphene and the surface oxygen are hybridized near the Fermi level. The

Table 1 – The magnetic moment of each atoms in the isolated MgO (111) surface and graphene on the MgO (111) interface. The unit of the magnetic moment is μ_B.

	NM substrate	FM substrate	Ferrimagnetic interface
Oxygen	0	0.4	0.16
Bonded Carbon	–	–	−0.06
Unbonded Carbon	–	–	0.17

carbon has an additional covalent bond with the surface oxygen, and the surface oxygen can occupy only one sublattice of the graphene due to its periodicity. It indicates that the sp3 hybridization state carbon is periodically included on only one sublattice side of the graphene. The sp3 hybridized carbon atoms can be a scattering point for the graphene and break the translational symmetry of the sublattice. Such symmetry breaking of the subattice is also observed in the LEED experiment of graphene on MgO (111) [32]. The breaking of the translational symmetry results in the creation of localized states at the Fermi level, where additional electrons or holes are injected to the defect [52]. The localized state only allows a spin-polarized state because of the local electron–electron interaction [53]. For this reason, similar magnetism was also observed in vacancy or hydrogen chemisorption in the graphene, depending on the sublattice symmetry [54,55]. Therefore, the substrate sp3 state of the graphene also shows spin-polarization.

In the graphene on the MgO (111), the spin-polarization was not localized at the bonded carbon, but delocalized to the entire graphene as shown in Fig. 6(a). The atoms in the sublattice containing sp3 hybridization showed a negative magnetic moment, while the atoms in the other sublattice showed a positive magnetic moment. The PDOS of each sublattice of the graphene on MgO (111) are plotted in Fig. 6(b). In the graphene on MgO (111), the sublattice containing sp3 hybridized carbon does not have many states near the Fermi-level.

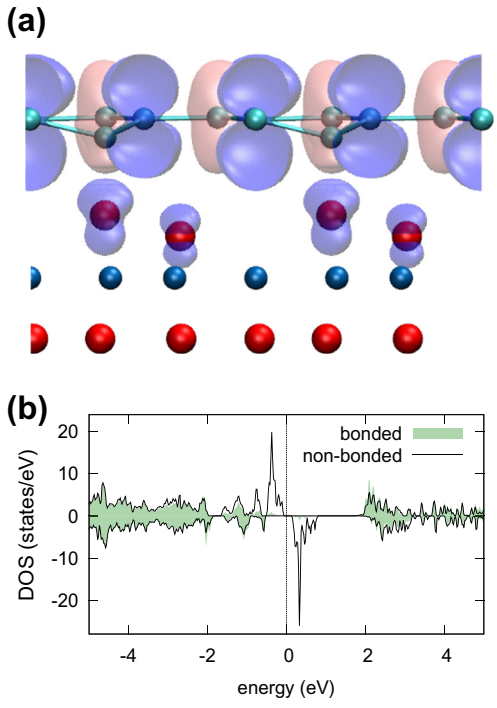

Fig. 6 – (a) The spatial spin density difference ($\rho_\uparrow - \rho_\downarrow$) of the graphene on ($\sqrt{3} \times \sqrt{3}$) MgO (111). The isovalues for the blue and red isosurfaces are 0.01 and −0.01 e/Å^3, respectively. The bonded sublattice forms a minority-spin channel, while the surface oxygen and non-bonded sublattice possess a majority-spin channel. (b) Shows the sum of the PDOS of the carbon atoms in each sublattice of the graphene. Below the Fermi level, the PDOS of the bonded sublattice was remarkably decreased, compared to the non-bonded sublattice. (A colour version of this figure can be viewed online.)

A substrate-induced sp2-sp3 alternative structure can induce spin-polarized bandgap. The effect of the alternative structure can be characterized by the effect of the covalent bond in one sublattice and the effect of the spin-degeneracy breaking between the two sublattices. When the covalent bond is introduced to graphene, the band of the graphene can be shifted [56]. This occurs because of the energy offset between the substrate and the graphene. Furthermore, the covalent bond decouples the π-electron from one sublattice of the graphene, and the induced local imbalance between the two sublattices causes the bandgap. When the spin-degeneracy of the two sublattices is broken, it also induces inequivalency in the sublattices for either spin projection. Because of the exchange interaction and the many-body effect, such an inequivalency results in a spin-polarized band near the Fermi level [57]. The electrons whose spin is parallel (antiparallel) to the net magnetic moment has an energetically favored (unfavored) band. Considering the similarities between a majority-spin band in a range from −3 to −1 eV and a minority-spin band in a range from −1 to 1 eV, it is deduced that a spin polarized bandgap was formed by shifting and splitting of the band. Therefore, it is believed that the origin of the spin-polarized bandgap is a substrate-induced sp2-sp3 alternative bonding and related spin-ordering.

4. Conclusions

In conclusion, the spin-polarized semiconducting property of graphene is achieved by using a substrate effect with ($\sqrt{3} \times \sqrt{3}$) MgO (111), which induces an sp2-sp3 alternative bonding structure to graphene. The spin-polarized bandgap can generate a spin-polarized current, which opens up a number of avenues for practical applications of graphene to spintronics. These findings suggest that substrate engineering can be a highly effective method for the tuning of graphene electronic structures. The realization of graphene-based spintronics can be achieved by tailor-made substrate engineering with fine control of the surface magnetism and periodicity for the interface bonding.

Acknowledgments

This work was supported by a National Research Foundation (NRF) Grant funded by the Korean Ministry of Science, ICT & Future Planning (No. 2011-0016945), Basic Science Research Program through the NRF of Korea funded by the Ministry of Education (No. 2013R1A1A2A10064432) and the project of Global Ph.D Fellowship conducted by the NRF in 2011 (No. 2011-0007330).

Appendix A. Supplementary data

Supplementary data associated with this article can be found, in the online version, at http://dx.doi.org/10.1016/j.carbon.2014.05.023.

REFERENCES

[1] Wolf S, Awschalom D, Buhrman R, Daughton J, Von Molnar S, Roukes M, et al. Spintronics: a spin-based electronics vision for the future. Science 2001;294(5546):1488–95.
[2] Žutić I, Fabian J, Sarma SD. Spintronics: fundamentals and applications. Rev Mod Phys 2004;76(2):323.
[3] Pesin D, MacDonald AH. Spintronics and pseudospintronics in graphene and topological insulators. Nat Mater 2012;11(5):409–16.
[4] Tombros N, Jozsa C, Popinciuc M, Jonkman H, Van Wees B. Electronic spin transport and spin precession in single graphene layers at room temperature. Nature 2007;448(7153):571–4.
[5] Avsar A, Yang T-Y, Bae S, Balakrishnan J, Volmer F, Jaiswal M, et al. Toward wafer scale fabrication of graphene based spin valve devices. Nano Lett 2011;11(6):2363–8.
[6] Cobas E, Friedman AL, van't Erve OMJ, Robinson JT, Jonker BT. Graphene as a tunnel barrier: graphene-based magnetic tunnel junctions. Nano Lett 2012;12(6):3000–4.
[7] Kim WY, Kim KS. Prediction of very large values of magnetoresistance in a graphene nanoribbon device. Nat Nanotechnol 2008;3(7):408–12.
[8] Maassen J, Ji W, Guo H. Graphene spintronics: the role of ferromagnetic electrodes. Nano Lett 2011;11(1):151–5.
[9] Son YW, Cohen ML, Louie SG. Half-metallic graphene nanoribbons. Nature 2006;444(7117):347–9.
[10] Kan E, Li Z, Yang J, Hou JG. Half-metallicity in edge-modified zigzag graphene nanoribbons. J Am Chem Soc 2008;130(13):4224–5.
[11] Deng X, Zhang Z, Tang G, Fan Z, Yang C. Spin filter effects in zigzag-edge graphene nanoribbons with symmetric and asymmetric edge hydrogenations. Carbon 2014;66(0):646–53.
[12] Zhou J, Wang Q, Sun Q, Chen XS, Kawazoe Y, Jena P. Ferromagnetism in semihydrogenated graphene sheet. Nano Lett 2009;9(11):3867–70.
[13] Liu Y-S, Wang X-F, Chi F. Non-magnetic doping induced a high spin-filter efficiency and large spin seebeck effect in zigzag graphene nanoribbons. J Mater Chem C 2013;1(48):8046–51.
[14] Park H, Wadehra A, Wilkins JW, Neto AHC. Spin-polarized electronic current induced by sublattice engineering of graphene sheets with boron/nitrogen. Phys Rev B 2013;87(8):085441.
[15] Felser C, Fecher GH, Balke B. Spintronics: a challenge for materials science and solid-state chemistry. Angew Chem Int Ed 2007;46(5):668–99.
[16] Fiederling R, Keim M, Reuscher Ga, Ossau W, Schmidt G, Waag A, et al. Injection and detection of a spin-polarized current in a light-emitting diode. Nature 1999;402(6763):787–90.
[17] Jonker BT, Erwin SC, Petrou A, Petukhov AG. Electrical spin injection and transport in semiconductor spintronic devices. MRS Bull 2003;28(10):740–8.
[18] Zhu H, Ramsteiner M, Kostial H, Wassermeier M, Schönherr H, Ploog K, et al. Room-temperature spin injection from fe into gaas. Phys Rev Lett 2001;87(1). p. 016601–016601.
[19] Hanbicki AT, Jonker B, Itskos G, Kioseoglou G, Petrou A. Efficient electrical spin injection from a magnetic metal/tunnel barrier contact into a semiconductor. Appl Phys Lett 2002;80(7):1240–2.
[20] Ohno Y, Young D, Beschoten Ba, Matsukura F, Ohno H, Awschalom D. Electrical spin injection in a ferromagnetic semiconductor heterostructure. Nature 1999;402(6763):790–2.
[21] Jansen R. Spintronics: solar spin devices see the light. Nat Mater 2013;12(9):779–80.
[22] Dash SP, Sharma S, Patel RS, de Jong MP, Jansen R. Electrical creation of spin polarization in silicon at room temperature. Nature 2009;462(7272):491–4.
[23] Jansen R. Silicon spintronics. Nat Mater 2012;11(5):400–8.
[24] Kittilstved KR, Liu WK, Gamelin DR. Electronic structure origins of polarity-dependent high-tc ferromagnetism in oxide-diluted magnetic semiconductors. Nat Mater 2006;5(4):291–7.
[25] Schwartz DA, Gamelin DR. Reversible 300 k ferromagnetic ordering in a diluted magnetic semiconductor. Adv Mater 2004;16(23–24):2115–9.
[26] Pearton S, Abernathy C, Overberg M, Thaler G, Norton D, Theodoropoulou N, et al. Wide band gap ferromagnetic semiconductors and oxides. J Appl Phys 2003;93(1):1–13.
[27] Jiang X, Wang R, Shelby R, Macfarlane R, Bank S, Harris J, et al. Highly spin-polarized room-temperature tunnel injector for semiconductor spintronics using mgo (100). Phys Rev Lett 2005;94(5):056601.
[28] Li Y, Chye Y, Chiang Y, Pi K, Wang W, Stephens J, et al. Inversion of ferromagnetic proximity polarization by mgo interlayers. Phys Rev Lett 2008;100(23):237205.
[29] Butler W, Zhang X-G, Schulthess T, MacLaren J. Spin-dependent tunneling conductance of fe—mgo—fe sandwiches. Phys Rev B 2001;63(5):054416.
[30] Parkin SS, Kaiser C, Panchula A, Rice PM, Hughes B, Samant M, et al. Giant tunnelling magnetoresistance at room temperature with mgo (100) tunnel barriers. Nat Mater 2004;3(12):862–7.
[31] Yuasa S, Nagahama T, Fukushima A, Suzuki Y, Ando K. Giant room-temperature magnetoresistance in single-crystal fe/mgo/fe magnetic tunnel junctions. Nat Mater 2004;3(12):868–71.
[32] Gaddam S, Bjelkevig C, Ge S, Fukutani K, Dowben PA, Kelber JA. Direct graphene growth on mgo: origin of the band gap. J Phys: Condens Matter 2011;23(7):072204.
[33] Cho SB, Chung YC. Bandgap engineering of graphene by corrugation on lattice-mismatched mgo (111). J Mater Chem C 2013;1(8):1595–600.
[34] Ciston J, Subramanian A, Marks LD. Water-driven structural evolution of the polar mgo (111) surface: an integrated experimental and theoretical approach. Phys Rev B 2009;79(8):085421.
[35] Tasker PW. The stability of ionic crystal surfaces. J Phys C 1979;12(22):4977. http://stacks.iop.org/0022-3719/12/i=22/a=036.
[36] Gajdardziska-Josifovska M, Crozier PA, Cowley JM. A (3×3) r30 reconstruction on annealed (111) surfaces of mgo. Surf Sci 1991;248(1):L259–64.
[37] Subramanian A, Marks LD, Warschkow O, Ellis DE. Direct observation of charge transfer at a mgo (111) surface. Phys Rev Lett 2004;92(2):26101.
[38] Kresse G, Furthmüller J. Efficient iterative schemes for ab initio total-energy calculations using a plane-wave basis set. Phys Rev B 1996;54(16):11169.
[39] Perdew J, Burke K, Ernzerhof M. Generalized gradient approximation made simple. Phys Rev Lett 1996;77(18):3865–8.
[40] Blöchl P. Projector augmented-wave method. Phys Rev B 1994;50(24):17953.
[41] Grimme S. Semiempirical gga-type density functional constructed with a long-range dispersion correction. J Comput Chem 2006;27(15):1787–99.
[42] Heaton RJ, Madden PA, Clark SJ, Jahn S. Condensed phase ionic polarizabilities from plane wave density functional theory calculations. J Chem Phys 2006;125:144104.
[43] Reckien W, Janetzko F, Peintinger MF, Bredow T. Implementation of empirical dispersion corrections to

density functional theory for periodic systems. J Comput Chem 2012;33:2023.
[44] Bucko T, Hafner J, Lebegue S, Angyán JG. Improved description of the structure of molecular and layered crystals: Ab initio dft calculations with van der waals corrections. J Phys Chem A 2010;114(43):11814–24.
[45] Huang B, Xu Q, Wei SH. Theoretical study of corundum as an ideal gate dielectric material for graphene transistors. Phys Rev B 2011;84(15):155406.
[46] Monkhorst HJ, Pack JD. Special points for Brillouin-zone integrations. Phys Rev B 1976;13(12):5188–92.
[47] Mattausch A, Pankratov O. Ab initio study of graphene on sic. Phys Rev Lett 2007;99(7):76802.
[48] Zhou SY, Gweon GH, Fedorov AV, First PN, De Heer WA, Lee DH, et al. Substrate-induced bandgap opening in epitaxial graphene. Nat Mater 2007;6(10):770–5.
[49] Du A, Sanvito S, Smith SC. First-principles prediction of metal-free magnetism and intrinsic half-metallicity in graphitic carbon nitride. Phys Rev Lett 2012;108(19):197207.
[50] Yoo JW, Chen CY, Jang HW, Bark CW, Prigodin VN, Eom CB, et al. Spin injection/detection using an organic-based magnetic semiconductor. Nat Mater 2010;9(8):638–42.
[51] Gallego S, Beltrán J, Cerdá J, Muñoz M. Magnetism and half-metallicity at the o surfaces of ceramic oxides. J Phys: Condens Matter 2005;17(43):L451.
[52] Červenka J, Katsnelson MI, Flipse CFJ. Room-temperature ferromagnetism in graphite driven by two-dimensional networks of point defects. Nat Phys 2009;5(11):840–4.
[53] Vozmediano MAH, López-Sancho MP, Stauber T, Guinea F. Local defects and ferromagnetism in graphene layers. Phys Rev B 2005;72(15):155121.
[54] Yazyev OV, Helm L. Defect-induced magnetism in graphene. Phys Rev B 2007;75(12):125408.
[55] Kumazaki H, Hirashima D. Nonmagnetic-defect-induced magnetism in graphene. Physica E 2008;40(5):1703–5.
[56] Wehling TO, Katsnelson MI, Lichtenstein AI. Impurities on graphene: midgap states and migration barriers. Phys Rev B 2009;80(8):085428.
[57] Daghofer M, Zheng N, Moreo A. Spin-polarized semiconductor induced by magnetic impurities in graphene. Phys Rev B 2010;82(12):121405.